



Photonics of Sub-Wavelength Nanowire Superlattices

Seokhyoung Kim*

Department of Chemistry, Northwestern University, Evanston, Illinois 60208, U.S.A.

ABSTRACT

Semiconductor nanowires (NWs) have widely been studied as an ideal platform for developing electronic, photovoltaic, photonic devices and biological probes in the nanoscale. The ability to synthesize high-quality NWs of various materials with a precise control in shape, doping and crystal structure is the key to the growth of NW-based technologies. In the past decade, there has been growing interest in controllably creating NW heterojunctions and periodically-modulated superlattices (SLs) because it is expected to bring new functionalities that are not present in uniform NWs. In particular, the interaction of NW SLs with light has been one of the central interests because the diameter and modulation length scale are on the same order as the wavelength of light in the optical regime. Also, degenerately-doped semiconductor NWs exhibit localized surface plasmon resonances (LSPRs), which comprises unexpected long-range interactions when the plasmon resonators are regularly placed in NW SLs. In this review, I will summarize the recent progress in photonics research of NW SLs. The topics discussed include preparation and types of NW SLs, light-trapping and light-emission properties, and plasmonic optical- and thermal-transport properties.

INTRODUCTION

Since the first discovery of vapor-liquid-solid (VLS) growth of nanowires (NWs) by Wagner and Ellis in 1964,[1] high-quality semiconductor NWs have grown into an important class of nanomaterials that exhibit useful properties and utilities in many different fields. Depending on the target application, NWs have been used as homogenous single crystals for optical Mie scattering and Fabry-Perot cavity oscillations, or with locally doped regions and carefully designed heterointerfaces for spatially-localized device structures such as NW *p-n* diodes, solar cells, and quantum-confined emitters. The development in NW synthesis has enabled the formation of heterostructures to controllably be directed either in the axial or radial direction, and the ability to design complex NW heterojunctions has generated a variety of device architectures in nanoelectronics,[2] photonics,[3] photovoltaics[4] and nano-bio interfaces.[5]

Initial demonstrations of NW growth modulation date back to the early 2000s,[2, 6] and it has thereafter evolved into a variety of NWs with repeated heterojunctions.[7] In particular, modulated NWs with precisely-tailored periodicity, defined as NW superlattices (SLs), have become an important research interest.[8-11] From an optical perspective, NWs with diameter on the order of 50-500 nm are an ideal platform that support well-defined Mie scattering in the visible and near-infrared (NIR) spectrum.[3] Moreover, when properly implemented in a periodic fashion, an axial modulation of physical quantities such as diameter, permittivity, and dopant concentration in this length scale is expected to give rise to new photonic, plasmonic, and hybrid[12] properties from NWs due to the formation of a photonic lattice.

In this review, I will attempt to summarize the emerging nanophotonic properties of NW SLs that have been studied within the past few years. I will first introduce the types of NW SLs with brief descriptions of their preparation methods. The following sections will discuss photonic properties of NW SLs that trap and emit light, and explain doping-enabled infrared (IR) plasmonic properties. I refer the interested readers to prior review/perspective articles[2-5, 7, 9] and references therein for more information about synthesis, growth kinetics, and applications in other areas.

TYPES OF NW SLs

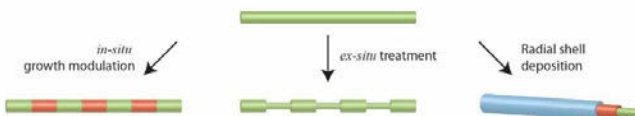


Figure 1. Synthetic routes to axial and radial NW SLs. Top: Uniform NW. Bottom left: Axial NW SL prepared by *in-situ* growth modulation. Shaded colors indicate segments with different chemical identities such as a crystal structure, composition, and doping concentration. Bottom middle: Axial NW SL with diameter modulation. Bottom right: Radial NW SL prepared by sequential shell deposition.

NW SLs can be prepared either by *in-situ* growth methods or through *ex-situ*, post-growth methods. The *in-situ* methods take advantage of the ability of the VLS process to rapidly change the growth environment through the control of growth parameters such as temperature, chamber pressure, and partial pressures of precursor gases and impurities. The growth perturbation typically results in an alteration of crystal

structures,[13-15] material compositions,[16-18] or dopant concentrations[8, 9] in individual NWs, as depicted in the bottom left of Figure 1. On the other hand, these NWs can also be placed under chemical treatments after growth terminates. In particular, subtractive treatments such as chemical etching tend to produce modulated external diameters[8, 9] (bottom middle, Figure 1), while additive treatments such as sequential deposition commonly put shells around them[19, 20] (bottom right, Figure 1).

NW SLs are commonly classified into axial and radial SLs based on the direction in which the modulation is made. Of the two, the axial geometry is of greater interest for designing nanophotonic devices because many nanophotonic properties arise from collective interference effects of regularly spaced resonators. Additionally, the length scale of periodicity in axial SLs may range from single to hundreds of nanometers depending on the properties looked for. For example, NW SLs for the design of quantum effects would require a period of a few nanometers. On the other hand, common design rules for photonic crystals (PCs) indicate that the size and spacing need to be on the order of the wavelength of light, for which periods of hundreds of nanometers are a more suited geometry.

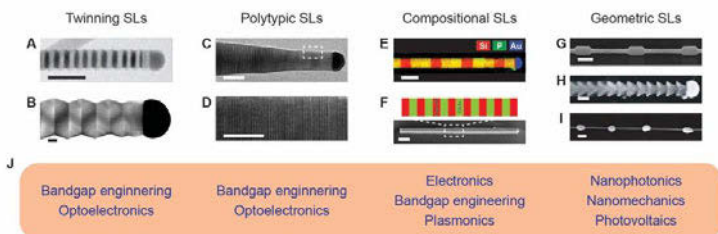


Figure 2. Types of axial NW SLs and their applicable areas of study. (A-B) Twinning NW SLs of InP (A) and GaAs (B) with periodic twin boundaries; scale bars, 50 nm (A) and 100 nm (B). (C) Polytypic NW SLs of InAs with an alteration of the crystal phase between WZ and ZB; scale bar, 40 nm. (D) Magnified view of a boxed region from (C); scale bar, 10 nm. (E-F) Compositional NW SLs showing a varying concentration of P dopant in a Si NW (E) and Sb in a GaAs NW (F); scale bars, 200 nm (E) and 1 μm (F). (G-H) Geometric SLs with periodically undulated diameters; scale bars, 200 nm. (I) Geometric SL with Ge islands periodically deposited on a Si NW through Plateau-Rayleigh crystal growth; scale bar, 200 nm. (J) Relevant areas of study for axial NW SLs. Reprinted with permission (A) from ref. 13, Copyright 2008 Springer Nature, (B) from ref. 14, Copyright 2013 American Chemical Society, (C-D) from ref. 22, 2010 American Chemical Society, (E) from ref. 23, Copyright 2017 American Chemical Society, (F) from ref. 17, Copyright 2018 American Chemical Society, (G) from ref. 9, Copyright 2016 American Chemical Society, (H) from ref. 26, Copyright 2015 The American Association for the Advancement of Science, (I) from ref. 27, Copyright 2015 Springer Nature.

Axial NW SLs are further divided into subclasses based on the physical/chemical nature of the modulation. Figure 2 shows four types of axial NW SLs: twinning, polytypic, compositional, and geometric SLs. Twinning SLs (TSLs) are NWs made of a single material with repeated twin boundaries. The lattice switching and formation of twin boundaries are typically triggered by the abrupt introduction of impurities and the surface tension of a liquid catalyst droplet at the liquid-solid interface, respectively. Algra et al.[13] reported that a higher partial pressure of diethylzinc, a *p*-type dopant for InP NWs, induced a reduction of a step energy of the zinc blende (ZB) lattice structure. The reduced formation energy of ZB caused the growth of ZB to be more favorable than wurtzite (WZ) lattice, the preferred crystal phase during unperturbed growth. They also found that above a certain partial pressure threshold, their ZB NWs

formed periodic twin planes because the shape of the front growth facet constantly changed due to the side facets, {111}A and {111}B, not being parallel to the growth direction. As a result, InP TSLs with a regular spacing were formed as presented in Figure 2A. A GaAs NW TSL formed by the same effect but with a much larger diameter[14] is presented in Figure 2B.

Likely, the crystal phase alteration itself can produce NW SLs, namely polytypic SLs (PSLs).[21, 22] Figure 2C shows a single InAs NW of which the crystal phase periodically switches between WZ and ZB.[22] Atomically-sharp transitions with no stacking faults were achieved by optimizing both temperature and the ratio of group-III and V materials. As seen in the magnified image (Figure 2D), the InAs PSL exhibits a defect-free alteration of eight-bilayer-thick segments of each crystal phase.

Introduction of dopants or additional elements is also used to create abrupt compositional transitions and to make NW compositional SLs (CSLs). At an optimal condition, the compositional modulation occurs without interrupting crystal structures. For example, doping silicon (Si) NWs in *n*- and *p*-types have been the fundamental control that enables the NW-based electronics technologies.[2, 4] Christesen et al. created Si NWs with a variety of complex doping profiles to the final lengths of tens of microns with high uniformity using a digital growth control.[8] In their following studies, the dopant transition was found as abrupt as 3-4 nm[23] as shown in Figure 2C, and both *n*- and *p*-type CSLs are developed.[24]

The compositional modulation is not limited to doping, but can also affect the elemental content of the main semiconductor materials, which can result in modification of band structures. III-V NWs are a popular platform for this type of CSLs because of a large variety of elemental combinations possible among group III and V elements, and due to their superior optoelectronic properties originated from having direct bandgaps. Altering precursors for group III and V elements directly translates to the composition of the corresponding elements in the NWs, as demonstrated with InAs/GaAs[16] NW CSLs for alteration of group III elements, and InP/InAs[18] for group V elements. In addition to complete switching of either group III or V elements, partial switching in an alloyed NW is also possible when a mixture of precursors is used. Figure 2D shows a GaAs/GaAsSb NW CSL in which the content of Sb oscillates along the NW axis.[17] The compositional modulation is also demonstrated with lead halide perovskite (LHPs) NWs. Dou et al. performed an anion exchange technique to produce $\text{CsPbBr}_3/\text{CsPbCl}_3$ NW CSLs, which exhibited spatially-resolved, multicolored photoluminescence (PL, Figure 4F).[25] The electronic and optical properties are discussed in detail in later sections.

Lastly, geometric SLs (GSLs) are NWs with an external diameter changing along the NW axis. GSLs are synthesized by removing materials from specific areas of uniform NWs, or depositing shells in a non-uniform, periodic manner. Using the dopant-dependent etch rate of *n*-type Si, Christesen et al.[8, 9] removed a portion of low-doped regions using potassium hydroxide (KOH) etchant to create Si NW GSLs (Figure 2E). The etch rate tendency of *n*-type Si can be reversed when etched in buffered hydrofluoric acid (BHF),[23] and NW GSLs with *p*-type Si NWs were later developed.[24] On the other hand, Lou et al.[26] have also demonstrated Si NW GSLs through a slightly different method without a dopant control. They deposited dense atomic Au coating around Si NWs by periodically evacuating the vacuum chamber during the growth, and the periodic Au shell served as an etch mask during the subsequent etch process (Figure 2F). Contrary to the subtractive methods, Day et al.[27] created NW GSLs by locally depositing shells on Si NWs. This was achieved by inducing the Plateau-Rayleigh (P-R) instability of the shells such that the shells broke into isolated islands in a periodic manner (Figure 2G). This method also allowed for the formation of heterojunctions between the core NW and P-R shells.

PHOTONIC NW SLS

Light trapping properties

One of the most intuitive photonic properties one can expect from a NW SL is a ‘grating-like’ interaction with light. Grating couplers diffract light to different angles, and couple a pitch-matched wavelength to the nearby waveguide. Unlike diffractive interactions by gratings, NWs interact with light through Mie resonances for which the spectral position is determined by the NW diameter. NW GSLs possess an additional set of resonances due to the axial lattice. The GSL modes are dependent on GSL pitch and exhibit asymmetric Fano lineshapes, similar to guided resonances found from PC slabs.[28] Thus, considering the origin of these optical modes, Mie and GSL resonances can be treated as diameter modes and guided modes, respectively. It is worth noting that the GSL *guided* modes are observed under normally-incident light illumination with a net zero wavevector, and exhibit a standing wave pattern formed by two counter-propagating guided modes. Consequently, they are often called *bound guided states* (BGSS) to differentiate them with conventional guided modes with definite wavevectors.[29] The GSL modes are distinct from the diffraction of grating couplers in a number of ways. The most important aspect is that the GSL modes are fundamentally governed by both Mie scattering and the waveguide theory of cylinders, which necessitates consideration of all geometric parameters, two diameters and pitch, in examining their properties.

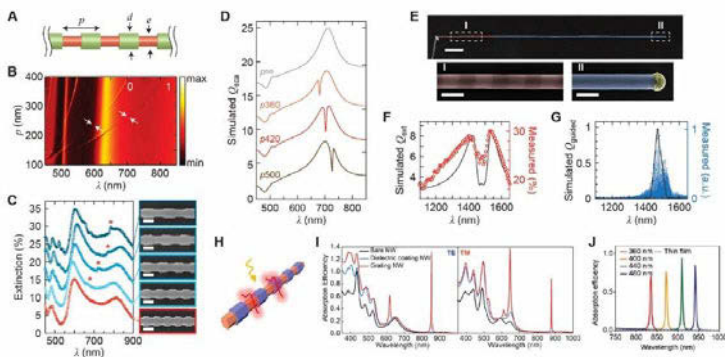


Figure 3. Light trapping in NW GSLs. (A) Schematic of a NW GSL with outer diameter (d), inner diameter (e) and pitch (p) where each segment length is $p/2$. (B) Scattering heatmap of a GSL showing vanishing points on sharp Fano branches in $m = 0$ and 1 angular channels. (C) Left: Measured extinction spectra of five GSLs with varying pitch. The Fano peak vanishes in the bottom-most spectrum. Spectra vertically offset by 5%. Right: Scanning electron microscope image of the GSLs used for the extinction measurements in the left panel; scale bars, 200 nm. (D) Q_{sca} of a uniform NW (denoted p^∞) showing a broad Mie resonance, and of GSLs showing sharp a Fano resonance tunable through pitch. Spectra offset by 5. (E) Top: False-colored SEM image of a NW containing a GSL (shaded in red) and straight WG (shaded in blue); scale bar, 5 μm . Bottom: Magnified views of boxed regions from the top panel; scale bars, 500 nm. (F-G) Simulated and measured extinction (F) and guided spectra (G) of a GSL from panel (E). (H) Si NW with a hexagonal cross-section and periodically spaced shell. (I) Calculated absorption efficiency of a bare NW and GSLs under TE- and TM-polarized plane wave illumination. (J) Shift of a sharp absorption peak of a Si NW GSL with varying pitch. Reprinted with permission (A-C) from ref. 30, Copyright 2019 American Physical Society, (D-G) from ref. 29, Copyright 2018 Springer Nature, (H-I) from ref. 34, Copyright 2016 The Optical Society, (J) from ref. 35, Copyright 2017 The Optical Society.

In their recent work, Kim et al.[30] demonstrated that NW GSLs can function as perfect optical cavities that confine optical energy for infinite lifetimes. The GSL modes they found exhibited much narrower linewidths and higher quality-factors (Q-factors) than typical Mie resonances, and were perfectly trapped within the structure with zero radiative decay rates through optical bound states in the continuum[31] (BICs). At BICs, GSL modes are decoupled from the radiation continua by either a symmetry mismatch or destructive interference,[32] and the optical energy does not escape into the free space. As a result, the Fano lineshapes vanish in the scattering heatmap. Figure 3B shows two sharp branches of GSL modes denoted with angular numbers of 0 and 1, and both branches show characteristic line-vanishing points at pitch (p) values of 237 and 262 nm, respectively. This phenomenon is experimentally characterized by single-NW extinction spectroscopy with Si GSLs of varying pitch (Figure 3C).

Interestingly, the research team has also found that the optical power stored in a Mie resonance can be transferred to a BGS of the GSL.[29] The energy transfer occurs when a coupling between the two otherwise-orthogonal modes, the Mie resonance and guided mode, is permitted by the periodicity of the GSL at a select wavelength. It manifests as a sharp dip on a Mie scattering peak in extinction spectra, implying that the optical energy is funneled into the guided mode at the dip position (Figure 3D). This interaction is tunable by changing the GSL pitch, and resembles that of metamaterials that exchange optical energy between a bright and dark state.[33] Because the wire geometry of the NW GSLs allows them to be used as optical circuit elements, narrow-band waveguiding through the selective coupling effect is experimentally demonstrated at the telecommunication spectrum where absorption loss is not present. A characteristic scattering dip is observed over a Mie resonance envelop (Figure 3F), and a narrow waveguide band is obtained at the wavelength where the scattering dip is observed (Figure 3G).

The spectrally selective light-trapping effect has also been studied in the context of enhancing absorption in Si NW photovoltaics. When the Mie-BGS interaction is tuned to the NIR region where absorption by Si is normally very weak, one can expect a highly enhanced absorption from the trapped mode of a GSL. Lee et al.[34] predicted narrow absorption peaks with high efficiency even above unity from both transverse-electric (TE) and transverse-magnetic (TM) polarized illumination where electric and magnetic fields are oriented perpendicular to the NW axis, respectively (Figure 3I). Similar to the case in Figure 3D, the absorption enhancement is expected to be highly tunable with a geometric control (Figure 3J).[35]

Light emission properties

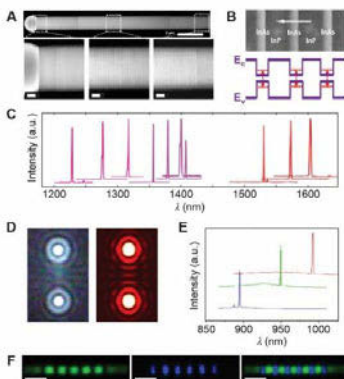


Figure 4. Light emission from NW SLs. (A) Top: Transmission electron microscope image of a InP/InAs MQW NW SL; scale bar, 2 μ m. Bottom: Magnified views of boxed regions from the top panel; scale bars, 200 nm. (B) MQW structure (top) and corresponding quantum-confined band diagram (bottom). (C) Tunable lasing in the telecommunication band region through quantum well thickness control. (D) Measured (left) and simulated (right) interference patterns of stimulated emission from a GaAs/GaAsSb MQW SL at room temperature. (E) Tunable lasing in the near-IR by controlling the Sb composition. (F) Confocal PL images of a CsPbX_3 NW SL where the halide alternates between Br and Cl. Green and blue colors correspond to the Br and Cl perovskite regions, respectively. Reprinted with permission (A-C) from ref. 18, Copyright 2019 The American Association for the Advancement of Science, (D-E) from ref. 17, Copyright 2018 American Chemical Society, (F) from ref. 25, Copyright 2017 National Academy of Sciences.

Luminescent and lasing properties in NW SLs are strictly speaking optoelectronic properties that involve band-to-band electronic transitions and quantum confinement engineering. This research topic is attracting increasing attention because of the small mode volume, spectral tunability, and versatile structural control. Taking advantage of the atomic precision of the VLS process, a number of NW CSLs exhibiting tunable lasing with multi-quantum-well (MQW) structures have recently been reported. Figure 4A shows scanning electron microscopy (SEM) images of a InP/InAs NW CSL containing 400 units of uniformly-spaced 9 nm-thick InAs quantum disks (QDs).[18] Its band structure is schematically depicted in Figure 4B where an amplified stimulated emission of telecommunication wavelength photons (Figure 4C) is expected from the QD regions. The tunable lasing in the visible and NIR regions can be simply achieved by switching to wider bandgap materials. Ren et al.[17] synthesized GaAs/GaAsSb NW CSLs that exhibited a tunable lasing action in this range (Figure 4D-E). Figure 4D shows the experimental and simulated interference patterns of coherent emission at the ends of NWs above the lasing threshold.

LHPs are another class of materials that exhibit superior electronic and photonic properties.[36] Their bandgap being tunable with the halide composition[37] makes them promising candidates for practical nanophotonic devices. In the past few years, a number of synthetic methods for LHP NWs have been developed in the solution and vapor phases.[36, 37] Dou et al.[25] combined a solution-phase synthesis with electron-beam lithography to create CsPbX_3 NWs with alternating bromide and chloride domains. Because of different bandgaps of the two domains, the resulting NW CSLs exhibited alternating green/blue PL colors (Figure 4F). The research team also

demonstrated heterojunctions of more than two components (not shown), a technique which offers opportunities for developing more complex device architectures.

PLASMONIC NW SLS

Localized surface plasmon resonances (LSPRs) are collective oscillations of free electrons in nanostructures excited by light waves, which concentrate high electric fields within a very small region. LSPRs provide means to get around the diffraction limit to achieve deep sub-wavelength focusing of light, and comprise important parts in areas such as optical computing and nanomedicine.[38-40] Noble metals are popular materials for LSPRs because they satisfy the high carrier concentration requirement ($> \sim 10^{23} \text{ cm}^{-3}$) for exhibiting plasmon resonances in the visible region.[40] However, LSPRs are not limited to noble metals, but degenerately-doped semiconductors with carrier density over 10^{20} cm^{-3} do exhibit plasmon resonances in the mid-infrared (MIR) and NIR regions.[40] VLS growth permits very high doping densities over this limit, and the ability to spatially localize the doped regions in NWs provides an ideal control to systematically study plasmonic properties of NW SLs.

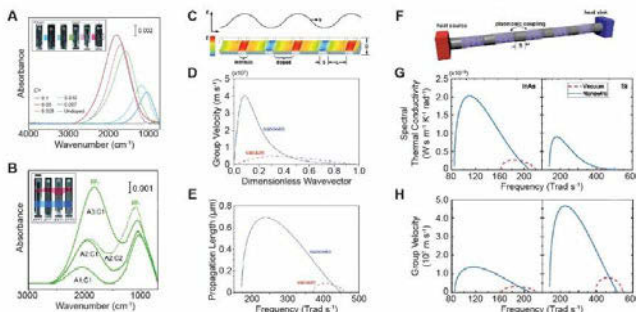


Figure 5. Plasmonic properties of doped NW SLs. (A) Dopant concentration dependence of a mid-IR LSPR of a Si NW. Inset: SEM images of NWs containing localized plasmonic segments visualized by dopant concentration-dependent buffered oxide etching; scale bar, 200 nm. (B) Bimodal surface plasmon coupling in single Si NWs. Inset: SEM images of NWs containing two localized plasmonic segments; scale bar, 200 nm. (C) Design of a NW plasmonic SL for deep sub-wavelength mid-IR waveguiding. (D-E) Calculated group velocity (D) and propagation length (E) of plasmonic waveguiding in periodic arrays of doped Si resonators embedded in a Si NW (solid blue curves) and in vacuum (dashed red curves). (F) Design of a NW plasmonic SL for photonic thermal conduction. (G-H) Spectral thermal conductivity (G) and group velocity (H) of SLs embedded in a NW (solid blue curves) and in vacuum (dashed red curves). Reprinted with permission (A-B) from ref. 41, Copyright 2013 John Wiley and Sons, (C-E) from ref. 43, Copyright 2018 The Royal Society of Chemistry, (F-H) from ref. 44, Copyright 2019 AIP Publishing.

Filler and his research team conducted several pioneering studies on LSPRs arising from highly doped Si NWs using controlled VLS growth equipped with *in-situ* infrared spectroscopy. In their early work, they observed a smooth blueshift of the LSPR peak position with increasing doping level within NW segments of the same aspect ratio (AR),[41] as shown in Figure 5A. They also studied the hybridization of LSPRs by encoding multiple plasmonic resonators in single NWs. The inset in Figure 5B shows NWs with two plasmon resonators of different parameters, and a characteristic bimodal splitting of two comprising LSPRs into ω_+ and ω_- is presented in Figure 5B.[41]

Interestingly, in their following study, they also found that, when the near-field coupling occurs between the two resonator segments, having the gap region filled with Si (due to the NW geometry) has a significant impact in the decay length and enhancement of the electric field compared to the gap being vacuum.[42] The decay length of the electric field in the intrinsic Si gap was increased by a factor of 4-5 compared to that of a vacuum gap, which resulted from the high IR permittivity of intrinsic Si. This finding inspired the design of plasmonic NW CSLs with periodically embedded MIR resonators for deep sub-wavelength MIR waveguiding (Figure 5C). With proper parameters, they predicted that the group velocities (Figure 5D) and propagation lengths (Figure 5E) of the waveguide modes are significantly higher for a NW CSL due to the stronger near-field coupling than an array of resonators in an isotropic vacuum environment.[43] Similarly, the team has also analyzed photonic thermal conduction in plasmonic CSLs (Figure 5F) using kinetic theory.[44] As opposed to photonic modes that do not contribute to thermal transport, it is predicted that plasmonic NW CSLs exhibit thermal conductivity up to $1 \text{ W m}^{-1} \text{ K}^{-1}$. This value is at least an order of magnitude higher than the maximum thermal conductivity thus far predicted for photonic counterparts.[44] These predictions for plasmonic NW CSLs bring opportunities for an extreme miniaturization of optical and thermal transport devices.

CONCLUSION AND OUTLOOK

The ability to create precise SL structures in semiconductor NWs has enabled a variety of new photonic, optoelectronic and plasmonic functionalities that do not naturally arise in bare NWs. The physical quantities that are discussed as control parameters include diameter, permittivity, bandgap, and carrier density. Understanding how these and potentially other physical quantities will dictate the properties of NW SLs will open up further opportunities for discovering interesting wave properties. Some of the work presented here are recent computational results that are being studied for experimental validations. Realizing these predictions in real systems will ultimately lead to the development of advanced device architectures in photovoltaics, solid-state lighting, optical on-chip technologies, and nanoscale photo-thermal management.

REFERENCES

- [1]. R. S. Wagner and W. C. Ellis, *Appl. Phys. Lett.* 4 (5), 89-90 (1964).
- [2]. M. S. Gudiksen, L. J. Lauhon, J. Wang, D. C. Smith and C. M. Lieber, *Nature* 415, 617 (2002).
- [3]. R. Yan, D. Gargas and P. Yang, *Nat. Photonics* 3 (10), 569-576 (2009).
- [4]. T. J. Kempa, R. W. Day, S.-K. Kim, H.-G. Park and C. M. Lieber, *Energy Environ. Sci.* 6 (3), 719-733 (2013).
- [5]. R. Parameswaran and B. Tian, *Acc. Chem. Res.* 51 (5), 1014-1022 (2018).
- [6]. M. T. Björk, B. J. Ohlsson, T. Sass, A. I. Persson, C. Thelander, M. H. Magnusson, K. Deppert, L. R. Wallenberg and L. Samuelson, *Nano Lett.* 2 (2), 87-89 (2002).
- [7]. L. Güniat, P. Caroff and A. Fontcuberta i Morral, *Chem. Rev.* 119 (15), 8958-8971 (2019).
- [8]. J. D. Christesen, C. W. Pinion, E. M. Grumstrup, J. M. Papanikolas and J. F. Cahoon, *Nano Lett.* 13 (12), 6281-6286 (2013).
- [9]. J. D. Christesen, C. W. Pinion, D. J. Hill, S. Kim and J. F. Cahoon, *J. Phys. Chem. Lett.* 7 (4), 685-692 (2016).
- [10]. I. R. Musin, N. Shin and M. A. Filler, *J. Mater. Chem. C* 2 (17), 3285-3291 (2014).
- [11]. L.-W. Chou, D. S. Boyuk and M. A. Filler, *ACS Nano* 9 (2), 1250-1256 (2015).

- [12]. C.-K. Chiang, Y.-C. Chung, P.-J. Cheng, C.-W. Wu, S.-W. Chang and T.-R. Lin, High Q/Vm hybrid photonic-plasmonic crystal nanowire cavity at telecommunication wavelengths. (SPIE, 2015).
- [13]. R. E. Algra, M. A. Verheijen, M. T. Borgstrom, L. F. Feiner, G. Immink, W. J. van Enckevort, E. Vlieg and E. P. Bakkers, *Nature* 456 (7220), 369-372 (2008).
- [14]. T. Burgess, S. Breuer, P. Caroff, J. Wong-Leung, Q. Gao, H. Hoe Tan and C. Jagadish, *ACS Nano* 7 (9), 8105-8114 (2013).
- [15]. S. Assali, J. Lähnemann, T. T. T. Vu, K. D. Jöns, L. Gagliano, M. A. Verheijen, N. Akopian, E. P. A. M. Bakkers and J. E. M. Haverkort, *Nano Lett.* 17 (10), 6062-6068 (2017).
- [16]. D. Scarpellini, C. Somaschini, A. Fedorov, S. Bietti, C. Frigeri, V. Grillo, L. Esposito, M. Salvalaglio, A. Marzegalli, F. Montalenti, E. Bonera, P. G. Medaglia and S. Sanguinetti, *Nano Lett.* 15 (6), 3677-3683 (2015).
- [17]. D. Ren, L. Ahtapodov, J. S. Nilsen, J. Yang, A. Gustafsson, J. Huh, G. J. Conibeer, A. T. J. van Helvoort, B.-O. Fimland and H. Weman, *Nano Lett.* 18 (4), 2304-2310 (2018).
- [18]. G. Zhang, M. Takiguchi, K. Tateno, T. Tawara, M. Notomi and H. Gotoh, *Sci. Adv.* 5 (2), eaat8896 (2019).
- [19]. T. J. Kempa, J. F. Cahoon, S.-K. Kim, R. W. Day, D. C. Bell, H.-G. Park and C. M. Lieber, *Proc. Natl. Acad. Sci.* 109 (5), 1407-1412 (2012).
- [20]. B. Tian, X. Zheng, T. J. Kempa, Y. Fang, N. Yu, G. Yu, J. Huang and C. M. Lieber, *Nature* 449 (7164), 885-889 (2007).
- [21]. P. Caroff, K. A. Dick, J. Johansson, M. E. Messing, K. Deppert and L. Samuelson, *Nat. Nanotechnol.* 4 (1), 50-55 (2009).
- [22]. K. A. Dick, C. Thelander, L. Samuelson and P. Caroff, *Nano Lett.* 10 (9), 3494-3499 (2010).
- [23]. S. Kim, D. J. Hill, C. W. Pinion, J. D. Christesen, J. R. McBride and J. F. Cahoon, *ACS Nano* 11 (5), 4453-4462 (2017).
- [24]. D. J. Hill, T. S. Teitsworth, S. Kim, J. D. Christesen and J. F. Cahoon, *ACS Appl. Mater. Interfaces* 9 (42), 37105-37111 (2017).
- [25]. L. Dou, M. Lai, C. S. Kley, Y. Yang, C. G. Bischak, D. Zhang, S. W. Eaton, N. S. Ginsberg and P. Yang, *Proc. Natl. Acad. Sci. U.S.A.* 114 (28), 7216-7221 (2017).
- [26]. Z. Luo, Y. Jiang, B. D. Myers, D. Isheim, J. Wu, J. F. Zimmerman, Z. Wang, Q. Li, Y. Wang, X. Chen, V. P. Dravid, D. N. Seidman and B. Tian, *Science* 348 (6242), 1451-1455 (2015).
- [27]. R. W. Day, M. N. Mankin, R. Gao, Y.-S. No, S.-K. Kim, D. C. Bell, H.-G. Park and C. M. Lieber, *Nat. Nanotechnol.* 10 (4), 345-352 (2015).
- [28]. S. Fan and J. D. Joannopoulos, *Phys. Rev. B* 65 (23), 235112 (2002).
- [29]. S. Kim, K.-H. Kim, D. J. Hill, H.-G. Park and J. F. Cahoon, *Nat. Commun.* 9 (1), 2781 (2018).
- [30]. S. Kim, K.-H. Kim and J. F. Cahoon, *Phys. Rev. Lett.* 122 (18), 187402 (2019).
- [31]. C. W. Hsu, B. Zhen, A. D. Stone, J. D. Joannopoulos and M. Soljačić, *Nat. Rev. Mater.* 1, 16048 (2016).
- [32]. E. N. Bulgakov and A. F. Sadreev, *Phys. Rev. A* 96 (1), 013841 (2017).
- [33]. N. Liu, L. Langguth, T. Weiss, J. Kästel, M. Fleischhauer, T. Pfau and H. Giessen, *Nat. Mater.* 8, 758 (2009).
- [34]. H.-C. Lee, J.-Y. Na, Y.-J. Moon, J.-S. Park, H.-S. Ee, H.-G. Park and S.-K. Kim, *Opt. Lett.* 41 (7), 1578-1581 (2016).
- [35]. J. S. Choi, K.-H. Kim and Y.-S. No, *Opt. Express.* 25 (19), 22750-22759 (2017).
- [36]. S.-T. Ha, R. Su, J. Xing, Q. Zhang and Q. Xiong, *Chem. Sci.* 8 (4), 2522-2536 (2017).
- [37]. H. Zhu, Y. Fu, F. Meng, X. Wu, Z. Gong, Q. Ding, M. V. Gustafsson, M. T. Trinh, S. Jin and X. Y. Zhu, *Nat. Mater.* 14, 636 (2015).
- [38]. N. J. Halas, S. Lal, W.-S. Chang, S. Link and P. Nordlander, *Chem. Rev.* 111 (6), 3913-3961 (2011).
- [39]. G. Chen, I. Roy, C. Yang and P. N. Prasad, *Chem. Rev.* 116 (5), 2826-2885 (2016).
- [40]. J. M. Luther, P. K. Jain, T. Ewers and A. P. Alivisatos, *Nat. Mater.* 10, 361 (2011).
- [41]. L. W. Chou and M. A. Filler, *Angew. Chem. Int. Ed. Engl.* 52 (31), 8079-8083 (2013).

- [42]. D. S. Boyuk, L. W. Chou and M. A. Filler, ACS Photonics 3 (2), 184-189 (2016).
- [43]. E. J. Tervo, D. S. Boyuk, B. A. Cola, Z. M. Zhang and M. A. Filler, Nanoscale 10 (12), 5708-5716 (2018).
- [44]. E. J. Tervo, M. E. Gustafson, Z. M. Zhang, B. A. Cola and M. A. Filler, Appl. Phys. Lett. 114 (16), 163104 (2019).